analytical chemistry

pubs.acs.org/ac Article

Imaging of Mitophagy Enabled by an Acidity-Reporting Probe Anchored on the Mitochondrial Inner Membrane

Shixiong Wen,[§] Xiao Hu,[§] Yilong Shi, Jiahuai Han, and Shoufa Han*

Cite This: *Anal. Chem.* 2021, 93, 16887−16898 Read Online

ACCESS | Metrics & More | Article Recommendations | Supporting Information

ABSTRACT: Classical chemical probes are prone to dissipation from stressed organelles, as evidenced by the incapability of mitochondrial dyes to image mitophagy linked to multiple diseases. We herein reported mitophagy imaging via covalent anchoring of a lysosomal probe to the mitochondrial inner membrane (**CALM**). Utilizing ^{DBCO}**RC-TPP**, an azide-conjugatable probe with acidity-triggered fluorescence, **CALM** is operated via ΔΨm-promoted probe accumulation in mitochondria and thereby bioorthogonal ligation of the trapped probe with azido-choline (^{Az}choline) metabolically installed on the mitochondrial membrane. Overcoming the limitation of synthetic probes to dissipate from stressed organelles, **CALM** enables signal-on fluorescence imaging of mitophagy induced by starvation and is further employed to reveal mitophagy in ferroptosis. These results suggest the potential of **CALM** as a new tool to study mitophagy.

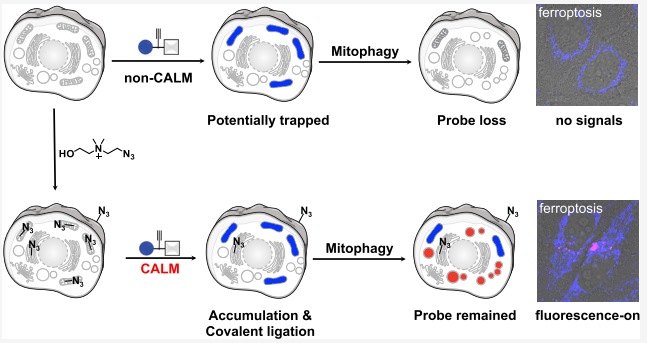

Mitophagy is an evolutionarily conserved degradation pathway by which excess or dysfunctional mitochondria are metabolized in lysosomes.[1−3] Critical for cell homeostasis and multiple human disorders, mitophagy has been intensively investigated for disease intervention,[4−7] which necessitates optical tracking of mitophagy.[8,9] Conventional cationic dyes accumulate in mitochondria, driven by mitochondrial membrane potential (ΔΨm), but are prone to dissipation from mitochondria upon ΔΨm loss.[10−12] This limits their use to track stressed mitochondria in mitophagy.[13,14] As such, researchers have coined various methods to immobilize synthetic probes in mitochondria, including covalent probe linking with mitochondrial proteins,[15−20] probe self-assembly,[21−24] and intraorganelle probe ligation.[25]

Recently, metabolic conversion of ^{Az}choline to azido-containing phosphatidylcholine was harnessed to immobilize optical probes to biological membranes via the bioorthogonal reaction.[26,27] Based on these advances, we sought to anchor an acidity-reporting probe into the mitochondrial inner membrane via bioorthogonal ligation with ^{Az}choline preinstalled in mitochondrial membranes, with the aim to image mitophagy by sensing pH acidification upon delivery of mitochondria into lysosomes (Scheme 1).

We opted to use a dibenzocyclooctyne (DBCO)-conjugated probe (^{DBCO}**RC-TPP**), which promptly accumulates in mitochondria and then combines ^{Az}choline preinstalled on the luminal membrane of mitochondria via stain-promoted azide-alkyne cyclization (SPAAC).[28] ^{DBCO}**RC-TPP** contains a moiety of triphenylphosphonium (TPP) to ensure prompt probe accumulation in mitochondria,[29−31] a DBCO moiety for covalent probe linking to ^{Az}choline-displaying membranes, a motif of coumarin with blue fluorescence to pinpoint mitochondria and an acidity-reporting motif of X-rhodamine-lactam (ROX-lactam) to given turn-on red fluorescence upon delivery of mitochondria into acidic lysosomes. Overcoming the liability of classical ΔΨm-sensitive dyes to dissipate from stressed mitochondria, **CALM** enabled dual-color tracking of mitophagy in cell starvation and was further employed to ascertain mitophagy during ferroptosis.

EXPERIMENTAL PROCEDURES

Materials and Methods. *Cell Lines, Plasmids, and Reagents.* HeLa (CCL-2), HT1080 (CCL-121), A549 (CCL-185), and MCF7 (HTB-22) cells were obtained from American Type Culture Collection (ATCC). LAMP2-GFP$^+$ HeLa and TOMM20-GFP$^+$ HeLa cells were prepared following the reported procedure.[32,33] All cell lines were cultured with Dulbecco's modified Eagle's medium (DMEM; GIBCO, C11995500CP) supplemented with 10% fetal bovine serum (Thermo, A3160901), 2 mM L-glutamine, 100 IU penicillin, and 100 mg/mL streptomycin at 37 °C in a humidified incubator under 5% CO_2.

Received: September 8, 2021
Accepted: December 2, 2021
Published: December 12, 2021

https://doi.org/10.1021/acs.analchem.1c03881
Anal. Chem. 2021, 93, 16887−16898

Scheme 1. CALM-Enabled Fluorescence-On Imaging of Mitophagy[a]

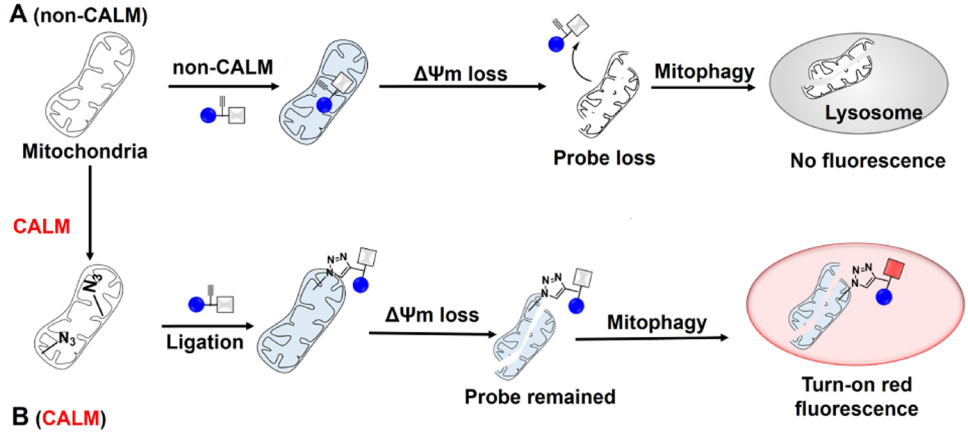

[a](A) Schematic for loss of conventional probes from stressed mitochondria in mitophagy. (B) Dual-color imaging of mitophagy with acidity-reporting ^{DBCO}RC-TPP linked to ^{Az}choline on the mitochondrial membrane. ^{DBCO}**RC-TPP** accumulates in mitochondria and forms covalent linkage with ^{Az}choline metabolically installed in the mitochondrial membrane, exhibiting blue fluorescence to pinpoint mitochondria. ^{DBCO}**RC-TPP** anchored in the mitochondrial membrane undergoes lysosomal acidity-triggered red fluorescence upon delivery of stressed mitochondria into acidic lysosomes, allowing signal-on imaging of mitophagy.

LysoTracker Green DND-26 (L7526) and MitoTracker Deep Red (M22426) were purchased from Invitrogen. Bafilomycin-A1 (Baf-A1; S1413), RSL3 (S8155), and Erastin (S7242) were purchased from Selleck. ^{Az}Choline was prepared following a reported literature procedure.[27] All other chemicals were purchased from Sigma unless specified.

Parkin-GFP-expressing and LAMP2-GFP-expressing plasmids were used for producing Parkin-GFP and LAMP2-GFP recombinant lentiviruses, respectively. Full-length cDNA of Parkin was cloned into BamHI and XhoI sites of the lentiviral vector pBOB-GFP using the ExoIII-assisted ligase-free cloning method. LAMP2-GFP-expressing plasmid and pMDLg, pRSV-REWV, pVSV-G, and pBOB-CMV vectors were gifts from Professor Jiahuai Han, Xiamen University. Recombinant lentiviruses were generated in 293 T cells (ATCC ACS-4500) in the presence of helper plasmids (pMDLg, pRSV-REWV, and pVSV-G) using a Lipofectamine 2000 reagent (Invitrogen, 11 668-019). All plasmids were verified by DNA sequencing. Expression of Parkin-GFP and LAMP2-GFP was validated by GFP fluorescence.

Microscopy. Fluorescence spectra were performed on SpectraMax M5 (Molecular Device). Confocal fluorescence microscopy imaging was performed on Zeiss LSM 780-2 using the following filters: λ_{ex} = 488 nm/λ_{em} = 499−553 nm for LysoTracker Green DND-26 and GFP, λ_{ex} = 561 nm/λ_{em} = 570−620 nm for MitoTracker Deep Red and ROX, and λ_{ex} = 405 nm/λ_{em} = 410−490 nm for coumarin.

Images of merged fluorescence were processed using ZEN 2 (blue edition). The graph was generated by GraphPad Prism 8 and origin 2019 software. Flow cytometry analysis was performed on BD Fortessa. The fluorescence emission intensity of coumarin was recorded by the BV421 filter (430−470 nm) using an excitation wavelength of 405 nm while that of ROX was recorded by PE-Texas Red (590−630 nm) using the excitation wavelength of 561 nm. The fluorescence of TOMM20-GFP was detected by the fluorescein isothiocyanate (FITC) filter (515−545 nm) using the excitation wavelength of 488 nm. Ten thousand cells were gated under identical conditions, analyzed, and the data were processed by FlowJo V10 software. All of the cells analyzed by confocal microscopy were seeded in 35 mm glass-bottom cell culture dishes.

Synthesis of ^{DBCO}RC-TPP (Scheme S1, Supporting Information). *Synthesis of Compound* ***2****.* To the solution of 2H-1-benzopyran-3-carboxylic acid (5.0 g, 19 mmol) in dichloromethane (DCM, 125.0 mL) were added 1-(3-dimethylaminopropyl)-3-ethylcarbodiimide hydrochloride (EDC, 4.7 g, 24.5 mmol) and *N*-hydroxysuccinimide (NHS, 2.9 g, 25.2 mmol). The reaction mixture was stirred at room temperature for 6 h, followed by addition of *N*-[(1,1-dimethylethoxy) carbonyl]-L-lysine (5.7 g, 22.8 mmol) and triethylamine (TEA, 8.0 mL). The reaction mixture was stirred at room temperature for 8 h and then washed with saturated aqueous solution of $NaHCO_3$ (125.0 mL). The organic layer was dried over anhydrous sodium sulfate and then concentrated by rotary evaporation. The residue was purified by silica gel column chromatography using CH_2Cl_2/MeOH (10/1) as the eluent to afford compound **2** in an overall 70% yield (6.6 g). ^{1}H NMR (500 MHz, $CDCl_3$) δ 9.27 (s, 1H), 8.64 (s, 1H), 7.38 (d, J = 8.9 Hz, 1H), 6.59 (d, J = 8.8 Hz, 1H), 6.42 (s, 1H), 4.86 (s, 1H), 4.63 (s, 1H), 3.41 (q, J = 7.2 Hz, 4H), 3.12 (q, J = 7.3 Hz, 1H), 3.07 (d, J = 8.0 Hz, 2H), 2.03 (s, 1H), 2.00−1.92 (m, 1H), 1.50 (q, J = 6.4 Hz, 2H), 1.38 (s, 8H), 1.27 (t, J = 7.3 Hz, 2H), 1.20 (t, J = 7.1 Hz, 6H). ^{13}C NMR (126 MHz, $CDCl_3$) δ 162.33, 157.65, 152.38, 147.90, 131.06, 109.73, 108.40, 96.61, 77.30, 77.25, 77.05, 76.79, 45.08, 45.02, 40.48, 29.48, 28.45, 12.43, 8.52. HRMS (ES^+) calculated for $C_{25}H_{35}N_3O_7^+$ (M^+) m/z = 489.2475, found: 489.2404.

Synthesis of Compound ***5****.* Compound **3**[34] (500 mg, 0.95 mmol) and compound **4**[25] (420 mg, 0.95 mmol) were dissolved in CH_2Cl_2 (25.0 mL) containing TEA (0.4 mL). The reaction mixture was stirred at room temperature for 4 h, washed with an aqueous solution of sodium hydroxide (1 mol/L), and then dehydrated with Na_2SO_4. The organic layer was concentrated and the residue was purified by silica gel column chromatography (CH_2Cl_2/MeOH/TEA = 150/10/1) to give compound **5** in 62.5% yield (500 mg). ^{1}H NMR (500 MHz, $CDCl_3$) δ 8.45 (s, 1H), 8.12 (d, J = 7.9 Hz, 1H), 7.76−7.56 (m, 15H), 6.93 (d, J = 7.9 Hz, 1H), 5.95 (s, 2H), 3.59 (td, J = 12.8, 7.2 Hz, 2H), 3.39 (s, 6H), 3.19 (t, J = 5.8 Hz, 1H), 3.11

https://doi.org/10.1021/acs.analchem.1c03881
Anal. Chem. 2021, 93, 16887−16898

(t, J = 5.6 Hz, 3H), 3.05 (q, J = 5.6 Hz, 3H), 2.87 (s, 4H), 2.39 (dp, J = 29.2, 7.8, 6.5 Hz, 4H), 2.28 (t, J = 7.2 Hz, 1H), 2.05−1.94 (m, 4H), 1.88 (t, J = 7.1 Hz, 2H), 1.79 (h, J = 6.5 Hz, 3H), 1.69 (d, J = 7.9 Hz, 1H), 1.24 (s, 2H), 0.86 (t, J = 6.8 Hz, 1H). ^{13}C NMR (151 MHz, $CDCl_3$) δ 172.31, 171.00, 170.14, 154.62, 148.23, 143.64, 139.97, 135.11, 135.09, 134.52, 133.59, 133.52, 130.59, 130.50, 129.79, 129.49, 124.43, 123.67, 123.04, 118.44, 117.87, 117.35, 107.70, 105.15, 77.27, 77.06, 76.85, 66.28, 49.87, 49.44, 40.11, 39.58, 35.93, 35.27, 31.90, 31.39, 29.72, 29.70, 29.66, 27.22, 27.17, 26.35, 26.24, 21.96, 21.84, 21.81, 21.65, 21.45, 21.20, 14.12. HRMS (ES^+) calculated for $C_{58}H_{58}N_4O_5P^+$ (M^+) m/z = 921.4139, found: 921.4132.

Synthesis of Compound ***6***. To the solution of compound **5** (300 mg, 0.3 mmol) in DCM (10.0 mL) were added EDC (94.0 mg, 0.5 mmol) and NHS (57.0 mg, 0.5 mmol). The reaction solution was stirred at room temperature for 4 h and then washed with aqueous hydrochloric acid (1 M, 3 × 20.0 mL). The organic layer was dehydrated with Na_2SO_4 and concentrated by rotary evaporation to give crude NHS ester of compound **5** (**5-NHS**) as a white residue. Compound **2** (240 mg, 0.5 mmol) was dissolved in CH_2Cl_2 (8.0 mL) containing trifluoroacetic acid (TFA, 2.0 mL). The mixture was stirred at room temperature for 0.5 h and then concentrated in vacuo. The residue was dissolved in CH_2Cl_2 (10.0 mL). The organic solution was washed with saturated aqueous solution of $NaHCO_3$ (10.0 mL) and then dehydrated with Na_2SO_4. To the above organic solution were added **5-NHS** and TEA (0.15 mL). The mixture was stirred at room temperature for 6 h and then washed with aqueous hydrochloric acid (1 M, 3 × 20.0 mL) and dehydrated with Na_2SO_4. The organic layer was concentrated by rotary evaporation. The residue was purified by silica gel column chromatography using ethyl acetate/MeOH/TEA (100/10/1) as the eluent to give compound **6** in 70% yield (300 mg). ^{1}H NMR (500 MHz, $CDCl_3$) δ 8.63 (d, J = 18.3 Hz, 2H), 8.23 (s, 1H), 8.10−7.99 (m, 1H), 7.95 (d, J = 8.0 Hz, 1H), 7.80−7.65 (m, 15H), 7.36 (d, J = 8.9 Hz, 1H), 7.05 (d, J = 7.8 Hz, 1H), 6.59 (d, J = 9.8 Hz, 1H), 6.43 (s, 1H), 5.92 (d, J = 5.8 Hz, 2H), 5.28 (s, 3H), 4.43 (q, J = 5.6 Hz, 1H), 3.52 (s, 2H), 3.41 (q, J = 7.0 Hz, 4H), 3.31−3.21 (m, 3H), 3.12 (s, 5H), 3.09−3.03 (m, 4H), 2.87 (s, 5H), 2.43 (h, J = 7.4, 6.4 Hz, 3H), 2.26 (t, J = 7.0 Hz, 1H), 2.03−1.97 (m, 4H), 1.91−1.85 (m, 2H), 1.84−1.76 (m, 4H), 1.73 (q, J = 8.5, 7.6 Hz, 2H), 1.55 (q, J = 6.8, 6.3 Hz, 2H), 1.52−1.44 (m, 2H), 1.24 (s, 1H), 1.20 (t, J = 7.0 Hz, 6H). ^{13}C NMR (151 MHz, $CDCl_3$) δ 175.34, 172.05, 168.87, 165.82, 162.78, 162.55, 157.52, 155.79, 152.33, 148.26, 148.20, 147.77, 143.78, 136.30, 135.36, 135.34, 133.59, 133.53, 132.46, 131.01, 130.66, 130.58, 130.35, 124.25, 124.17, 121.19, 118.29, 117.72, 117.51, 110.73, 109.79, 108.38, 107.72, 104.48, 104.41, 96.52, 77.27, 77.06, 76.85, 66.30, 58.30, 55.41, 53.45, 49.85, 49.41, 45.03, 39.96, 39.52, 35.19, 32.88, 29.93, 29.70, 29.52, 29.31, 27.18, 27.16, 26.26, 26.15, 23.15, 22.69, 22.24, 21.92, 21.85, 21.40, 21.19, 18.45, 14.12, 12.44. HRMS (ES^+) calculated for $C_{78}H_{83}N_7O_9P^+$ (M^+) m/z = 1292.5984, found: 1292.5982.

Synthesis of Compound ***8***. To a flask containing compound **6** (150.0 mg, 0.12 mmol), compound **7**[25] (33,0 mg, 0.13 mmol), and pyridine (5.0 mL) was added EDC (33.0 mg, 0.17 mmol). The reaction mixture was stirred at ambient temperature overnight and then concentrated. The residue was dissolved in CH_2Cl_2 (15.0 mL) and the solution was washed with aqueous hydrochloric acid (1 M, 15.0 mL). The organic layer was concentrated and the residue was separated by preparative TLC CH_2Cl_2/MeOH (40/1) to give compound **8** in 39% yield (70.0 mg). ^{1}H NMR (600 MHz, $CDCl_3$) δ 8.85−8.75 (m, 1H), 8.66 (d, J = 6.1 Hz, 1H), 7.76 (td, J = 13.1, 6.8 Hz, 11H), 7.69−7.61 (m, 8H), 7.38−7.30 (m, 4H), 7.12−7.03 (m, 2H), 6.63−6.56 (m, 1H), 6.44 (s, 1H), 5.93 (q, J = 5.5 Hz, 2H), 3.72−3.66 (m, 2H), 3.62 (s, 4H), 3.42 (d, J = 7.5 Hz, 5H), 3.24−3.20 (m, 2H), 3.11 (s, 3H), 3.05 (s, 3H), 2.92−2.90 (m, 2H), 2.88−2.85 (m, 2H), 2.56 (d, J = 7.9 Hz, 1H), 2.36 (s, 2H), 2.28 (d, J = 6.7 Hz, 2H), 2.19 (t, J = 7.7 Hz, 1H), 2.01−1.98 (m, 4H), 1.96 (s, 2H), 1.94 (s, 1H), 1.90−1.86 (m, 2H), 1.80 (s, 4H), 1.64 (d, J = 7.7 Hz, 1H), 1.61−1.57 (m, 2H), 1.40 (t, J = 7.3 Hz, 3H), 1.31 (s, 1H), 1.26 (s, 2H), 1.23 (s, 6H), 1.22−1.21 (m, 2H), 1.20 (s, 4H), 1.14 (t, J = 7.3 Hz, 1H), 1.10 (t, J = 7.3 Hz, 1H), 0.85 (t, J = 6.9 Hz, 2H). ^{13}C NMR (151 MHz, $CDCl_3$) δ 157.59, 152.47, 148.17, 148.04, 143.80, 135.03, 134.97, 133.74, 133.71, 133.67, 133.64, 130.49, 130.41, 129.76, 124.28, 118.61, 118.04, 117.53, 109.93, 108.43, 107.75, 104.27, 96.51, 70.57, 49.86, 49.41, 45.84, 45.05, 35.39, 34.47, 31.93, 31.91, 31.44, 29.77, 29.70, 29.66, 29.62, 29.53, 29.50, 29.37, 29.33, 29.27, 29.22, 29.13, 27.22, 27.18, 27.14, 23.35, 22.69, 21.91, 21.82, 21.39, 21.21, 14.86, 14.13, 12.45, 8.65, 1.02. HRMS (ES^+) calculated for $C_{96}H_{97}N_9O_9P^+$ (M^+) m/z = 1551.7175, found: 1551.7178.

In Vitro SPAAC of ^{DBCO}***RC-TPP*** *and* ^{Az}*Choline*. To the solution of ^{Az}choline (1.2 mg, 0.004 mmol) in CH_3OH (0.2 mL) was added ^{DBCO}**RC-TPP** (3.1 mg, 0.002 mmol). The reaction solution was mixed for 0.5 h at room temperature and then analyzed by HPLC and mass spectrometry. HRMS (ES^+) calculated for $C_{102}H_{113}N_{13}O_{10}P^{3+}$ (M^{3+}) m/z = 1710.8455/3 = 570.6163, found: 570.5437.

pH Titration. ^{DBCO}**RC-TPP** or its adduct with ^{Az}choline was dissolved in methanol to give a stock solution (100 μM). A portion of the stock solution of ^{DBCO}**RC-TPP** or adduct of ^{DBCO}**RC-TPP**/^{Az}choline stock solution was added to phosphate-buffered saline (PBS, 10 mM) containing methanol (30% v/v) of pH 4.0, 4.5, 5.0, 5.5, 6.0, 6.5, 7.0, 7.5, 8.0, 8.5, and 9.0 to a final concentration of 10 μM. The solution was analyzed for fluorescence emission.

Selectivity of ^{DBCO}***RC-TPP*** *for Mitochondria in TOMM20-GFP*$^+$ *HeLa Cells*. TOMM20-GFP$^+$ HeLa cells were cultured in DMEM with ^{Az}choline (500 μM, 24 h), then washed three times with PBS, and incubated with ^{DBCO}**RC-TPP** (2 μM, 1 h). The cells (referred to as **CALM**$^+$ cells) were washed with PBS and then imaged by confocal fluorescence microscopy.

Selectivity of ^{DBCO}***RC-TPP*** *in Additional Cell Lines*. A549, HT1080, and MCF7 cells were cultured with ^{Az}choline (500 μM, 24 h), washed three times with PBS, and then stained with ^{DBCO}**RC-TPP** (2 μM, 1 h). These cells were washed with PBS and then maintained in DMEM spiked with MitoTracker Deep Red (MTDR, 500 nM, 15 min) and then analyzed by confocal microscopy.

^{DBCO}***RC-TPP*** *Retention Detection in Stressed* ^{Az}*Choline*$^+$ *Mitochondria*. TOMM20-GFP$^+$ HeLa cells were cultured in DMEM without ^{Az}choline for 24 h, washed three times with PBS, and then stained with ^{DBCO}**RC-TPP** (2 μM, 1 h); these cells were referred to as **CALM**$^-$ cells. **CALM**$^+$ and **CALM**$^-$ HeLa cells were maintained in DMEM containing CCCP (25 μM, 1 h) or with no addition (control). In parallel, **CALM**$^+$ and **CALM**$^-$ MCF7 cells were stained with MitoTracker Deep Red (500 nM, 15 min). Then, the cells were washed three times with PBS and further cultured in DMEM containing CCCP (25 μM, 1 h) or with no addition. The resultant cells were analyzed by confocal fluorescence microscopy without washing (to maintain the levels of CCCP during analysis).

https://doi.org/10.1021/acs.analchem.1c03881
Anal. Chem. 2021, 93, 16887−16898

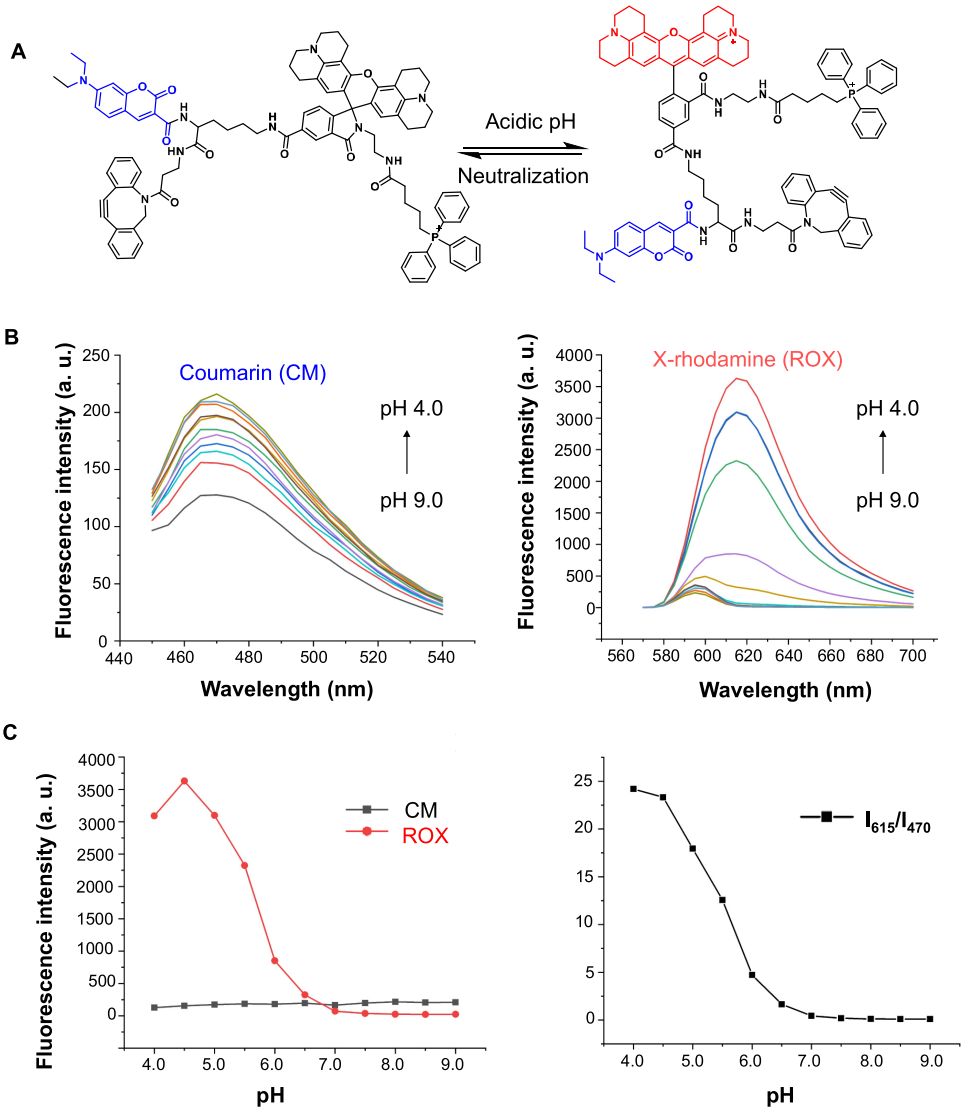

Figure 1. Optical properties of ^{DBCO}**RC-TPP**. (A) Acidity-triggered fluorogenic isomerization of ^{DBCO}**RC-TPP**. (B) Fluorescence emission of ^{DBCO}**RC-TPP**. ^{DBCO}**RC-TPP** was added to PBS buffer of pH 4.0−9.0 to a final concentration of 10 μM. The solutions were analyzed for fluorescence emission using λ_{ex} = 430 nm for coumarin and λ_{ex} = 595 nm for ROX. (C) pH titration curves of ^{DBCO}**RC-TPP**. The curves were plotted using fluorescence emission of ROX (I_{615} nm) and that of coumarin (I_{470} nm) over pH.

Temporal Retention of ^{DBCO}RC-TPP in Stressed CALM$^+$ and CALM$^-$ HeLa Cells. **CALM$^+$** and **CALM$^-$** HeLa cells were washed three times with PBS and maintained in DMEM containing CCCP (25 μM, 1 h), and then the cells were washed twice with PBS and harvested. The cells were centrifuged once and suspended in DMEM containing CCCP (25 μM) after removing the supernatant. The resultant cells were analyzed by flow cytometry. The fluorescence emission intensity of coumarin was recorded by the BV421 filter (430−470 nm) using the excitation wavelength of 405 nm.

Temporal Retention of ^{DBCO}RC-TPP in CALM$^+$ and CALM$^-$ HeLa Cells. **CALM$^+$** and **CALM$^-$** HeLa cells were cultured in fresh DMEM for 0 or 24 h, respectively, and then analyzed for intracellular coumarin fluorescence intensity by confocal fluorescence microscopy and flow cytometry.

Cytotoxicity Assay. HeLa cells were cultured for 24 h with no addition (control cells) or with ^{Az}choline (500 μM, referred to as ^{Az}choline$^+$ cells), and washed with PBS twice. Both cell samples were incubated with ^{DBCO}**RC-TPP** (2 μM, 1 h) or with no addition. These cells were seeded in a 96-well plate and then further cultured in fresh DMEM for 0, 24, and 48 h. The resultant cells were determined for cell viability by cell count kit 8 (MCE, hy-k0301) according to the manufacturer's guidance.

pH Profile of CALM in Live Cells. **CALM$^+$**/TOMM20-GFP$^+$ HeLa cells were incubated for 10 min in 4% formaldehyde at 37 °C. The fixed cells were washed twice with PBS, maintained for 1 h in high K$^+$ buffer (30 mM NaCl, 120 mM KCl, 1 mM $CaCl_2$, 0.5 mM $MgSO_4$, 1 mM NaH_2PO_4, 5 mM glucose [Sigma, G5764], 20 mM 4-(2-hydroxyethyl)-1-piperazineethanesulfonic acid (HEPES) [Sigma, H3375], 20 mM NaOAc [Sigma, S2889]) of various pH values (4.0, 5.0, 6.0, and 7.0), and then analyzed by confocal fluorescence microscopy.

Detecting Starvation-Induced Mitophagy with CALM. **CALM$^+$**/TOMM20-GFP$^+$ and **CALM$^+$**/LAMP2-GFP$^+$ HeLa cells were maintained for 6 h in fresh DMEM (control), Hanks' balanced salt solution (HBSS), or HBSS containing Baf-A1 (50 nM) and then analyzed by confocal fluorescence microscopy.

https://doi.org/10.1021/acs.analchem.1c03881
Anal. Chem. 2021, 93, 16887−16898

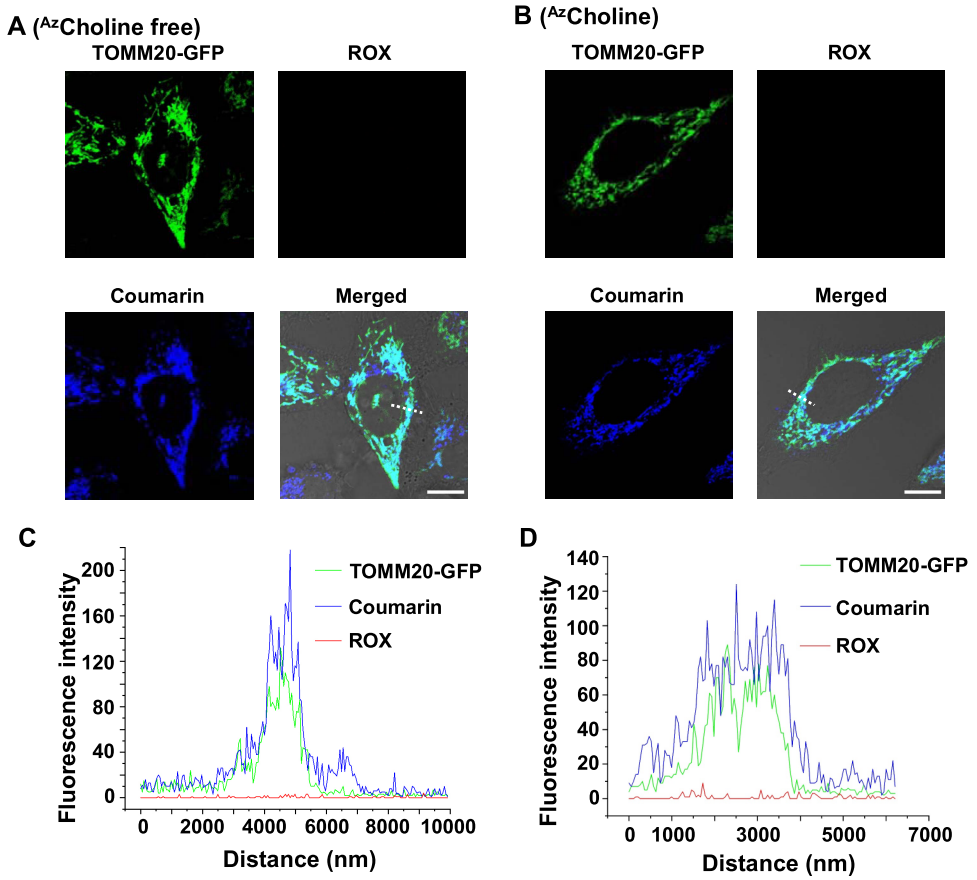

Figure 2. Selectivity of ^{DBCO}**RC-TPP** for mitochondria. TOMM20-GFP$^+$ HeLa cells precultured with no addition (A) or with ^{Az}choline (500 μM, 24 h) (B) were washed three times with PBS, stained with ^{DBCO}**RC-TPP** (2 μM, 1 h), and then imaged by confocal microscopy. Scale bar: 10 μm. Plots of fluorescence of coumarin, ROX, and TOMM20-GFP measured along the line shown in merged images of ^{Az}choline$^-$ cells (C) or ^{Az}choline$^+$ (D). This reveals colocalization of ^{DBCO}**RC-TPP** with TOMM20-GFP.

Imaging of Mitophagy in Parkin-Expressing Cells by CALM. **CALM**$^+$/Parkin-GFP$^+$ HeLa cells were incubated with CCCP (10 μM, 6 h) and then analyzed by confocal fluorescence microscopy. **CALM**$^+$ wild-type HeLa cells were incubated with LysoTracker Green DND-26 (LTG-DND266, 500 nM, 30 min); after washing with PBS, the cells were treated with CCCP (10 μM, 6 h) and then analyzed by confocal fluorescence microscopy. Control cells were maintained for 6 h in DMEM and then imaged.

Identifying Mitophagy in Ferroptosis Cells with CALM. **CALM**$^+$/LAMP2-GFP$^+$ and **CALM**$^+$/wild-type HT1080 cells were treated with no addition, with erastin (10 μM, 24 h), or with RSL3 (1 μM, 4 h) and then analyzed by confocal fluorescence microscopy.

Imaging of Mitophagy in Erastin-Sensitive Cells with CALM. **CALM**$^+$ and **CALM**$^-$ A549 cells were treated with no addition, with erastin (10 μM, 24 h), or with RSL3 (1 μM, 4 h), and then the cells were analyzed by confocal fluorescence microscopy without washing.

RESULTS AND DISCUSSION

Synthesis and Characterization of ^{DBCO}RC-TPP. Phospholipids are abundant constituents of organelle membranes.[35] ^{Az}Choline can be metabolically converted into azido-containing phospholipids which distribute into various biological membranes,[26] yielding a unique chemical handle installed on a biological membrane for further elaboration. Recently, visualization of organelle membrane trafficking was achieved via organelle-specific probes that are ligated to ^{Az}choline preinstalled in membranes after probe accumulation inside the organelles.[27]

Mitophagy is featured by the delivery of mitochondria into acidic lysosomes. However, efforts to image mitophagy with ΔΨm-sensitive pH sensors are inherently hampered by their tendency to dissipate from stressed mitochondria.[10] We envisioned that covalent linking of a ΔΨm-sensitive pH sensor with ^{Az}choline installed in the mitochondrial membrane could prevent leakage of imaging agents from stressed mitochondria in mitophagy. As such, we coined ^{DBCO}**RC-TPP**, a multifunctional probe comprised of a domain of coumarin with pH-inert blue fluorescence, TPP to target mitochondria, DBCO for bioorthogonal ligation to ^{Az}choline, and a domain of ROX-lactam fluorogenic to lysosomal acidity.[34] Synthesized via a five-step procedure in an overall 20% yield (Scheme S1, Supporting information), ^{DBCO}**RC-TPP** readily combined with ^{Az}choline in vitro to give the desired adducts in nearly quantitative yields, as evidenced by mass spectrometry (Figure S1, Supporting information). pH titration confirmed that ^{DBCO}**RC-TPP** and its adducts with ^{Az}choline exhibit pH-inert blue fluorescence and intense red fluorescence in acidic media with a calculated pK_a of 5.52 (Figures 1 and S2), which is consistent with protonation-mediated fluorogenic isomerization of ROX-lactam (Figures 1A and S2A).

https://doi.org/10.1021/acs.analchem.1c03881
Anal. Chem. 2021, 93, 16887−16898

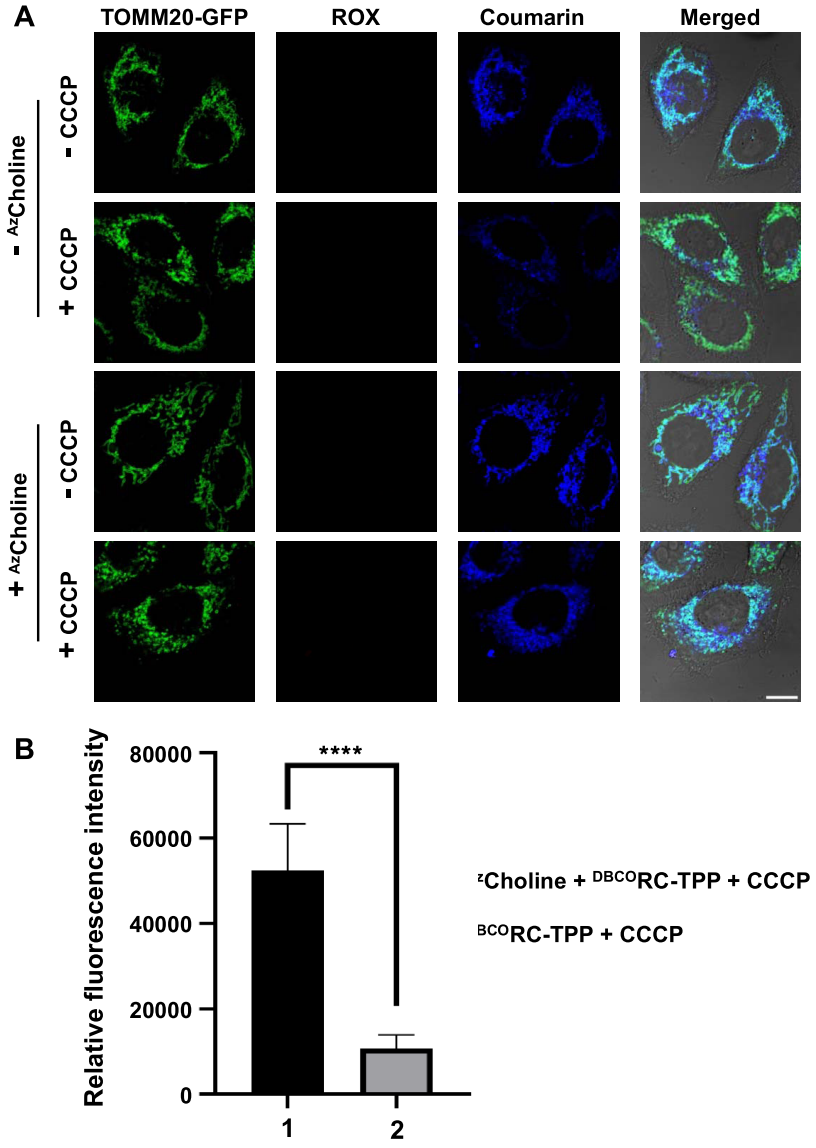

Figure 3. CALM-mediated fluorescence tagging of stressed mitochondria with ^{DBCO}**RC-TPP**. (A) Retention of ^{DBCO}**RC-TPP** in ^{Az}choline^{+}/TOMM20-GFP^{+} HeLa cells upon loss of ΔΨm. TOMM20-GFP^{+} HeLa cultured with or without ^{Az}choline were washed three times with PBS and then stained with ^{DBCO}**RC-TPP** (2 μM, 1 h). These cells were maintained in DMEM with or without CCCP (25 μM, 1 h) and then visualized by confocal microscopy. Scale bar: 10 μm. (B) Flow cytometric analysis on intracellular blue fluorescence of ^{Az}choline^{+}/^{DBCO}**RC-TPP**$^{+}$/CCCP^{+} cells over ^{DBCO}**RC-TPP**$^{+}$/CCCP^{+} cells (mean ± standard deviation, SD, n = 5000, ****P < 0.0001, unpaired Student's t-test).

Selectivity of ^{DBCO}RC-TPP for Mitochondria and Retention of ^{DBCO}RC-TPP in ^{Az}Choline^{+} Mitochondria. To achieve **CALM**, we first ascertained the selectivity of ^{DBCO}**RC-TPP** for mitochondria. HeLa cells expressing TOMM20-GFP^{+} were cultured with no addition (control) or with ^{Az}choline to metabolically install the azide moiety into overall subcellular membranes and then incubated with ^{DBCO}**RC-TPP**. Both **CALM**$^{-}$ and **CALM**$^{+}$ HeLa cells exhibited stringent probe colocalization with TOMM20-GFP, a constitutive protein of mitochondria (Figure 2). Probe targeting to mitochondria was also observed in additional **CALM**$^{+}$ cell lines including A549, HT1080, and MCF7 cells (Figure S3). Together, these data prove selective accumulation of ^{DBCO}**RC-TPP** in mitochondria.

To determine whether **CALM** could afford adducts trappable in ΔΨm-suppressed mitochondria, TOMM20-GFP^{+} HeLa cells cultivated with ^{Az}choline or with no addition were further stained with ^{DBCO}**RC-TPP**. These cells were washed with phosphate-buffered saline (PBS) and then treated with carbonyl cyanide *m*-chlorophenylhydrazone (CCCP) to dissipate ΔΨm.[36] CCCP caused dramatic attenuation of mitochondria-associated blue fluorescence in ^{Az}choline-free control cells (Figure 3A), a common feature of classical ΔΨm probes. In contrast, intense blue signals were revealed in mitochondria on TOMM20-GFP^{+}/^{Az}choline^{+} cells after CCCP treatment (Figure 3A), reflecting ^{Az}choline-mediated probe retention in CCCP-stressed mitochondria. Furthermore, flow cytometric analysis confirmed probe retention in CCCP-stressed mitochondria in ^{Az}choline^{+} cells over ^{Az}choline-free cells (Figure 3B). In addition, **CALM**-conferred fluorescence retention in stressed mitochondria also occurred in MCF7 cells (Figure S4).

We then performed time-course analysis on retention of ^{DBCO}**RC-TPP** in ^{Az}choline^{+} mitochondria relative to ^{Az}choline-free mitochondria, a parameter critical for long-term tracking of mitophagy. We cultured ^{DBCO}**RC-TPP**$^{+}$/^{Az}choline^{+} cells in

https://doi.org/10.1021/acs.analchem.1c03881
Anal. Chem. 2021, 93, 16887−16898

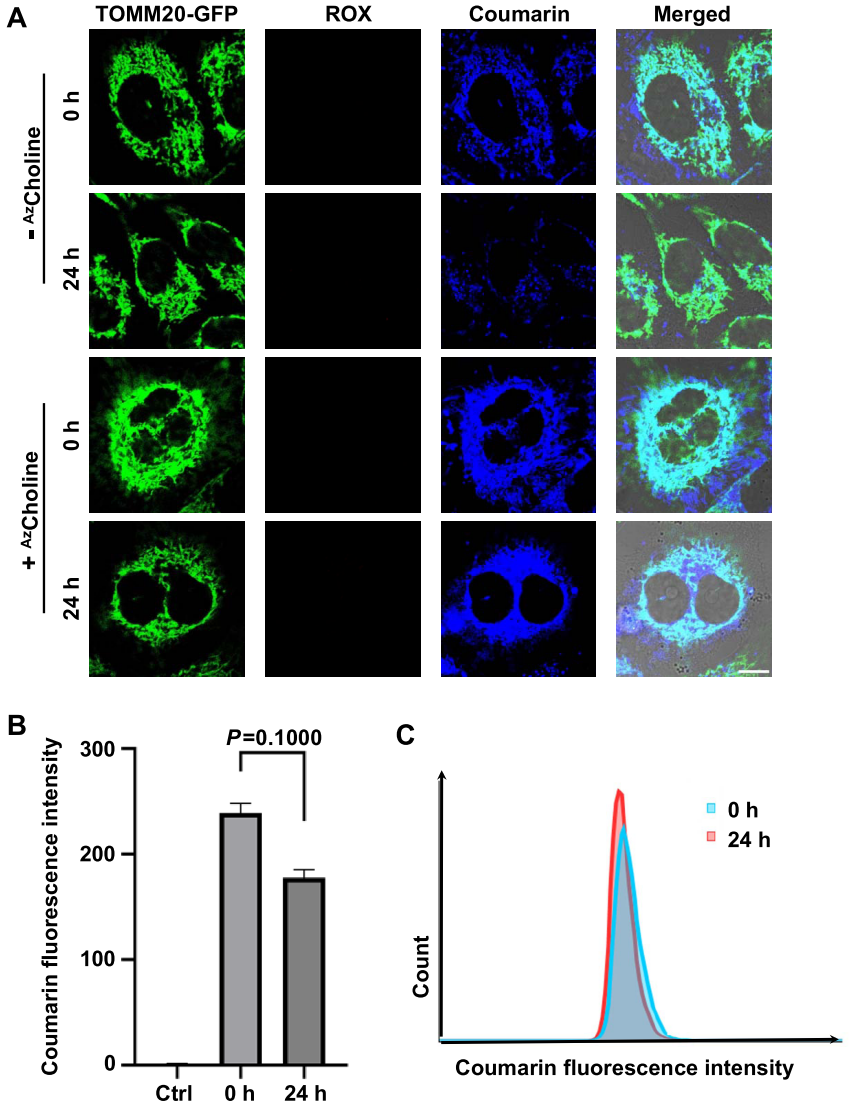

Figure 4. Long-term retention of ^{DBCO}**RC-TPP** in ^{Az}choline^{+} mitochondria. TOMM20-GFP^{+} HeLa cells precultured with or without ^{Az}choline were stained with ^{DBCO}**RC-TPP** (2 μM, 1 h). These cells were washed three times with PBS, maintained in fresh DMEM for 0 or 24 h, and then analyzed for intracellular fluorescence by confocal microscopy (A) and flow cytometry (B, C) (mean ± SD, n = 10 000, P > 0.05, unpaired Student's t-test). Scale bar: 10 μm.

fresh DMEM for 24 h and then assessed intracellular fluorescence by confocal microscopy and flow cytometry. We observed loss of ^{DBCO}**RC-TPP** fluorescence in HeLa cells free of ^{Az}choline whereas no loss of blue fluorescence could be detected in ^{Az}choline^{+} mitochondria (Figure 4), indicating long-term probe retention mediated by **CALM**. We at last assessed cytotoxicity of ^{DBCO}**RC-TPP** in HeLa cells and observed no detrimental effects on the vitality of Hela cells pretreated with or without ^{Az}choline (Figure S5). Combined, these findings showed that **CALM** could give rise to adducts stably trapped in ΔΨm-abolished mitochondria and thus the applicability of **CALM** for fluorescence tagging of stressed mitochondria.

Acidity-Triggered Red Fluorescence of ^{DBCO}RC-TPP Immobilized in ^{Az}Choline^{+}/^{DBCO}RC-TPP^{+} Mitochondria. To verify pH responsiveness of **CALM**, ^{Az}choline^{+}/^{DBCO}**RC-TPP**$^{+}$ cells were fixed with paraformaldehyde and then maintained in a buffer of varied pH values (pH 4−7). As expected, intracellular red fluorescence emerged in acidic pH and intensified as pH decreased (Figure 5), showing the feasibility of **CALM** to tag mitochondria with an acidity-reporting fluorogen.

Imaging of Mitophagy in Cell Starvation with CALM by Acidity-Triggered ROX Fluorescence. In mitophagy, the alkaline lumen of mitochondria (pH ∼ 8) is switched to acidic pH upon delivery of mitochondria into lysosomes (pH ∼ 4−5).[37] After validating the applicability of **CALM** to tag stressed mitochondria with acidity-reporting ^{DBCO}**RC-TPP**, we were keen to find out whether **CALM** could be used for dual-color imaging of mitophagy underlying multiple diseases.[38,39] We first assessed the specificity of **CALM** for mitophagy by starving TOMM20-GFP^{+} HeLa cells in Hanks' balanced salt solution (HBSS) for 6 h to induce mitophagy. Control cells free of starvation exhibited coumarin- and TOMM20-positive deposits, confirming probe accumulation in mitochondria, whereas starved cells displayed deposits of intense red fluorescence (Figure 6), indicating **CALM**$^{+}$ mitochondria in acidic lysosomes. We further confirmed that ROX fluorescence is specific for lysosomes by its colocalization with LysoTracker Green DND-26 (LTG-DND26) specific for lysosomes (Figure

https://doi.org/10.1021/acs.analchem.1c03881
Anal. Chem. 2021, 93, 16887−16898

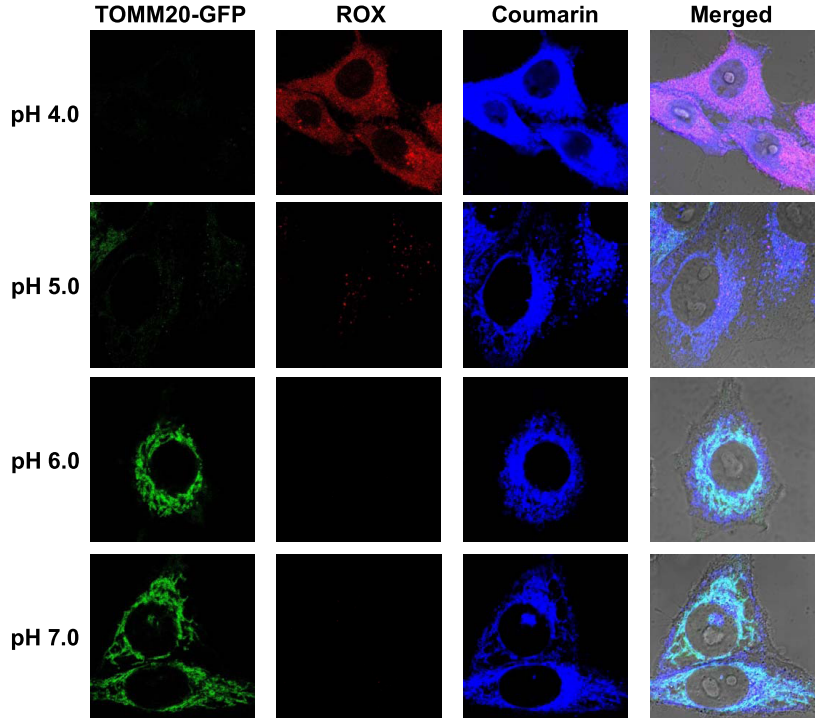

Figure 5. Acidity-triggered red fluorescence in ^{Az}choline^{+}/^{DBCO}RC-TPP^{+} cells. ^{Az}choline^{+}/^{DBCO}**RC-TPP**$^{+}$ HeLa cells were maintained for 1 h in high K^{+} buffer of diverse pH as indicated, and then imaged by confocal microscopy. Scale bar: 10 μm.

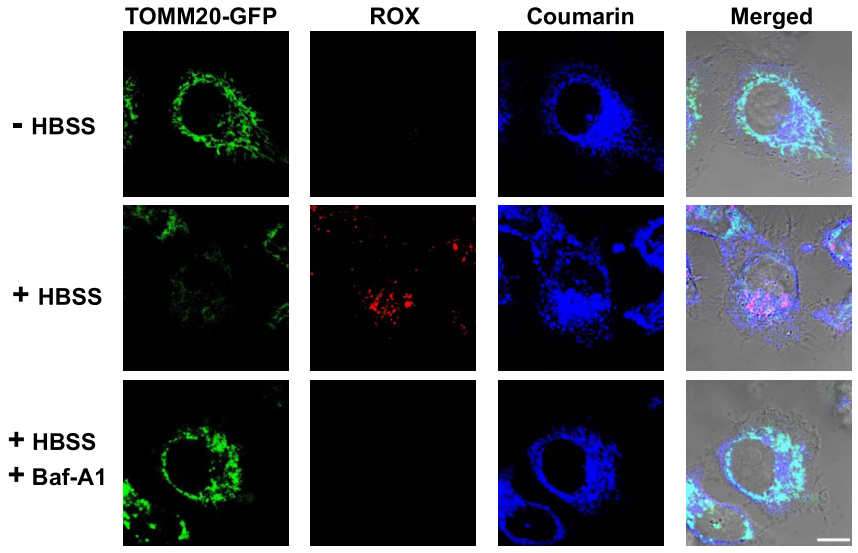

Figure 6. Imaging of starvation-induced mitophagy by **CALM. CALM**$^{+}$ cells were maintained for 6 h in HBSS, DMEM, or HBSS spiked with Baf-A1 (50 nM), respectively, and then visualized by confocal microscopy. Scale bar: 10 μm.

S6). Bafilomycin-A1 (Baf-A1) is a potent inhibitor of V-ATPase and effectively neutralizes lysosomes.[40] We found that the treatment of starved cells with Baf-A1 resulted in the loss of red fluorescence (Figure 6), reflecting lysosomal acidity-dependent red fluorescence.

To further validate mitophagy-mediated fluorescence activation, we applied **CALM** to discern mitophagy in HeLa cells expressing Parkin-GFP as compared to wild-type HeLa (W.T. HeLa) cells that exhibit low levels of mitophagy due to the lack of Parkin.[41] We identified significantly enhanced ROX signals induced by CCCP in Parkin-GFP^{+} cells over wild-type HeLa cells (Figure 7A,B). This is consistent with the role of Parkin in promoting mitophagy.[41] In addition, we observed the rise of red fluorescence over time in CCCP-treated cells and concurrent loss of Parkin-GFP signals due to degradation of Parkin-GFP by mitophagy (Figure 7A). Combined, these data support the selectivity of **CALM** for mitophagy imaging by lysosomal acidity-mediated turn-on red fluorescence. Given the recent advances on organelle-targeted dual-color probes,[42−44] the utility of **CALM** could be extended to image mitophagy by diverse biochemical species such as reactive oxygen species and acidic pH. Relative to one-step covalent linking of mitochondrial proteins relying on alkaline mitochondrial pH to alkylate thiols of mitochondrial proteins with nucleophilic probes, our method utilizes pH-independent bioorthogonal ligation to an anchor dual-color probe on the lipid membrane, offering an

https://doi.org/10.1021/acs.analchem.1c03881
Anal. Chem. 2021, 93, 16887−16898

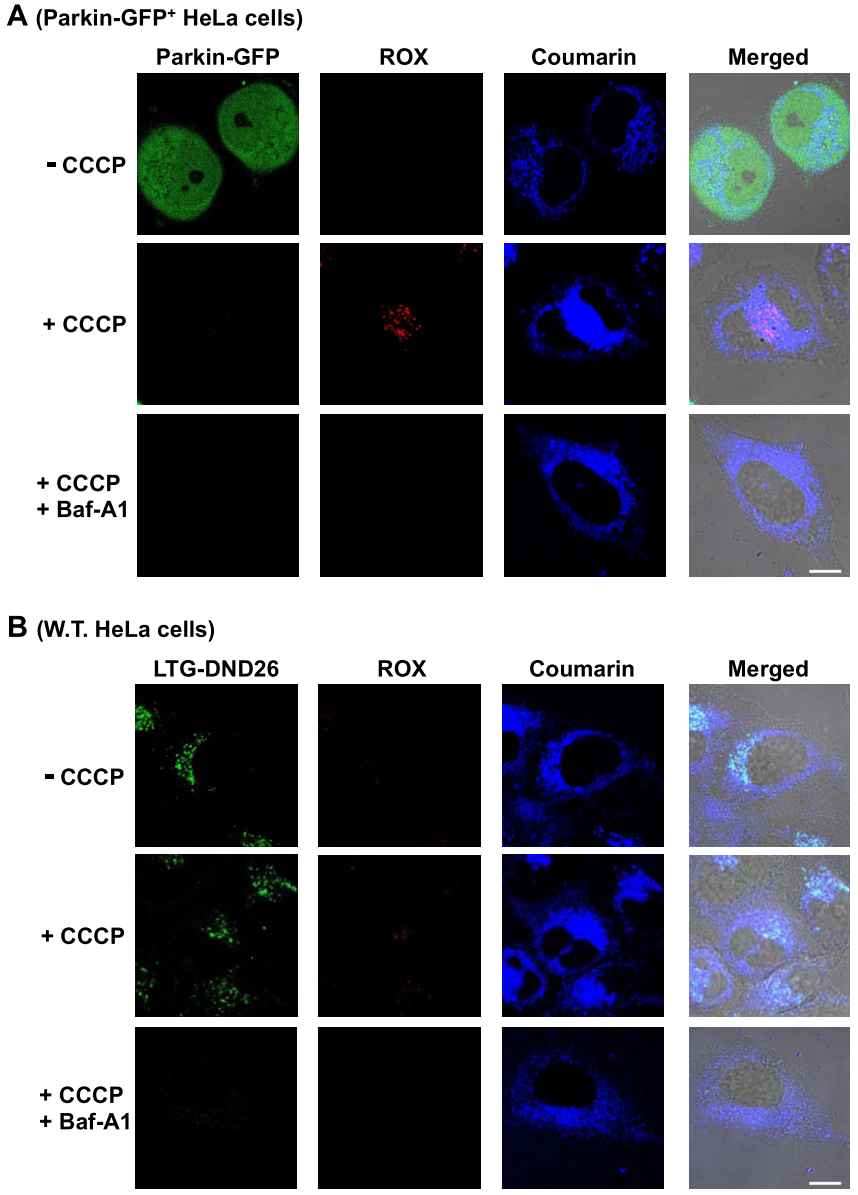

Figure 7. Parkin-enhanced mitophagy confirmed by **CALM**. (A) **CALM**$^{+}$/Parkin-GFP^{+} HeLa cells were treated for 8 h with no addition (control), CCCP (10 μM), or CCCP in combination with Baf-A1 (50 nM) before confocal microscopic analysis. (B) Wild-type HeLa cells were prestained with ^{DBCO}**RC-TPP** and LTG-DND26. These cells were further treated with no addition, with CCCP, or with CCCP/Baf-A1 for 8 h before analysis. Scale bar: 10 μm.

applicable method to tag stressed mitochondria of decreased pH.

Identifying Mitophagy in Ferroptosis with CALM. Ferroptosis is a regulated form of cell death engaged in multiple diseases.[45,46] Although mitophagy was reported to be important for ferroptosis,[47−51] controversial observation was also reported.[52] In addition, whether mitophagy occurs or not in ferroptosis remains poorly understood.[53,54] As mitochondria in ferroptosis exhibits alterations in morphology, integrity, and $\Delta\Psi$m loss,[55] we set to determine whether mitophagy occurred in ferroptosis. We applied **CALM** to HT1080 cells and then treated these cells with RSL3 or erastin,[56,57] which are classical ferroptosis inducers.[55] We detected red fluorescence in cells treated with both inducers whereas ROX signals are absent in control cells free of inducers (Figure 8A,B). We then applied **CALM** to HT1080 cells expressing LAMP2-GFP specific for lysosomes. Both RSL3 and erastin caused genesis of ROX fluorescence colocalized with LAMP2-GFP (Figure 9), indicating mitophagy induced under the assay conditions.

Because K-ras mutant A549 cells undergo erastin-induced ferroptosis but not RSL3-induced ferroptosis,[55] we treated **CALM**$^{+}$ A549 cells with erastin or RSL3. We observed bright red fluorescence on erastin^{+} A549 cells whereas no red fluorescence could be identified in RSL3^{+} A549 cells, showing mitophagy in ferroptosis. Finally, we analyzed cells undergoing ferroptosis with ^{DBCO}**RC-TPP** in the absence of ^{Az}choline and failed to observe any red fluorescence. These showed the critical role of **CALM** to identify mitophagy in ferroptosis (Figure 10). Together, these results support the occurrence of mitophagy during ferroptosis.

■ CONCLUSIONS

Defective mitophagy is engaged in multiple human diseases, but is elusive to image with conventional organelle probes

https://doi.org/10.1021/acs.analchem.1c03881
Anal. Chem. 2021, 93, 16887−16898

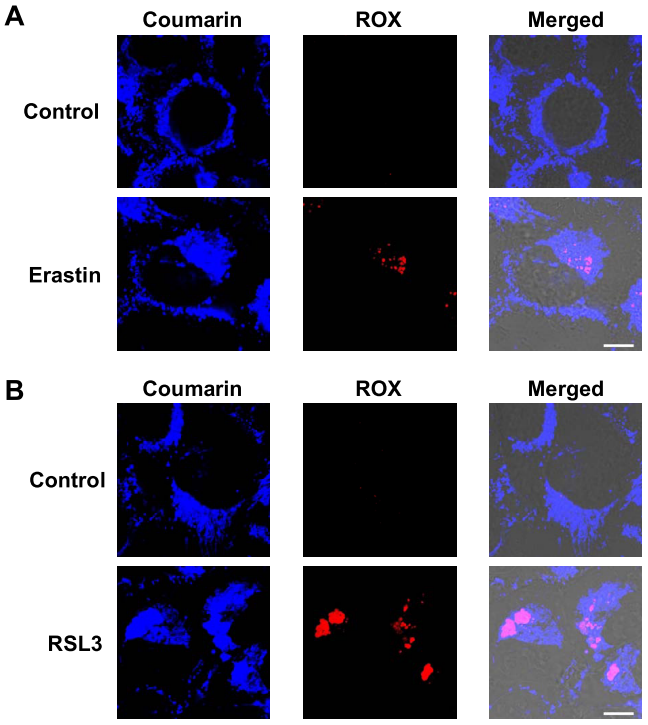

Figure 8. Imaging of mitophagy in ferroptosis by **CALM**. **CALM**$^{+}$ HT1080 cells were treated with erastin (10 μM, 24 h) (A) or with RSL3 (1 μM, 4 h) (B) to induce ferroptosis. Cells without erastin and RSL3 treatment were the control. All of the cells were analyzed by confocal microscopy. Scale bar: 10 μm.

owing to probe loss from damaged or stressed mitochondria. To overcome this, we herein report mitophagy imaging via covalent anchoring of a lysosomal probe to mitochondrial inner membrane (**CALM**), utilizing a lysosomal acidity-reporting probe (^{DBCO}**RC-TPP**) that is promptly partitioned in mitochondria and then bioorthogonally linked to ^{Az}choline metabolically incorporated into the mitochondrial membrane. **CALM** enables signal-on mitophagy detection via red fluorescence triggered upon delivery of mitochondria into lysosomes. We also applied **CALM** to identify mitophagy in

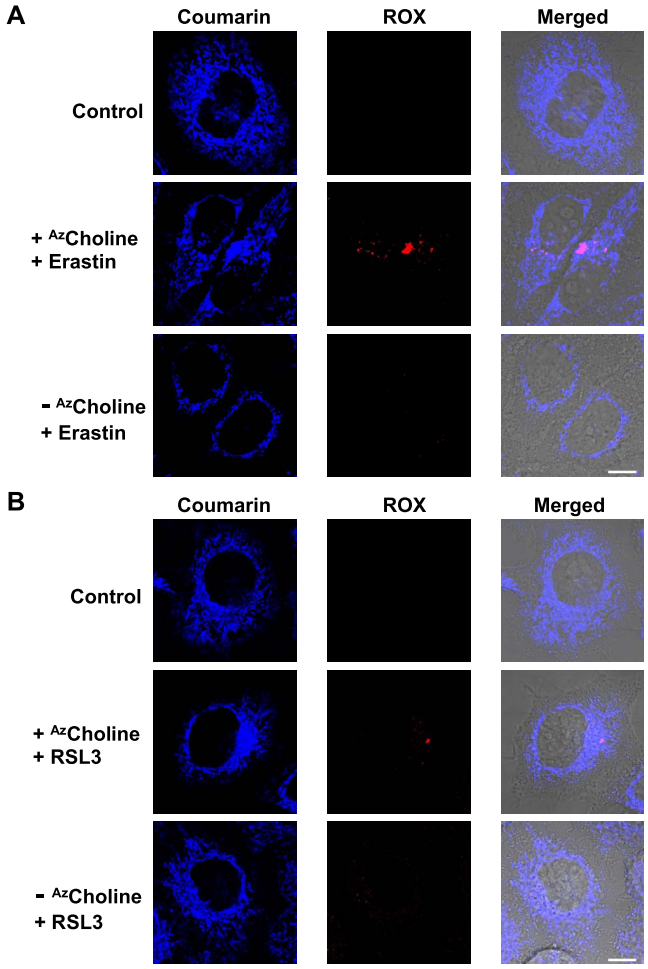

Figure 10. Dependence of red fluorescence on ferroptosis. K-ras mutant A549 cells precultured with or without ^{Az}choline were stained with ^{DBCO}**RC-TPP** and then treated with erastin (24 h, 10 μM) (A) or RSL3 (4 h, 1 μM) (B), respectively, before analysis by confocal microscopy. K-ras mutant A549 cells treated with ^{DBCO}**RC-TPP** alone were used as the control. Scale bar: 10 μm.

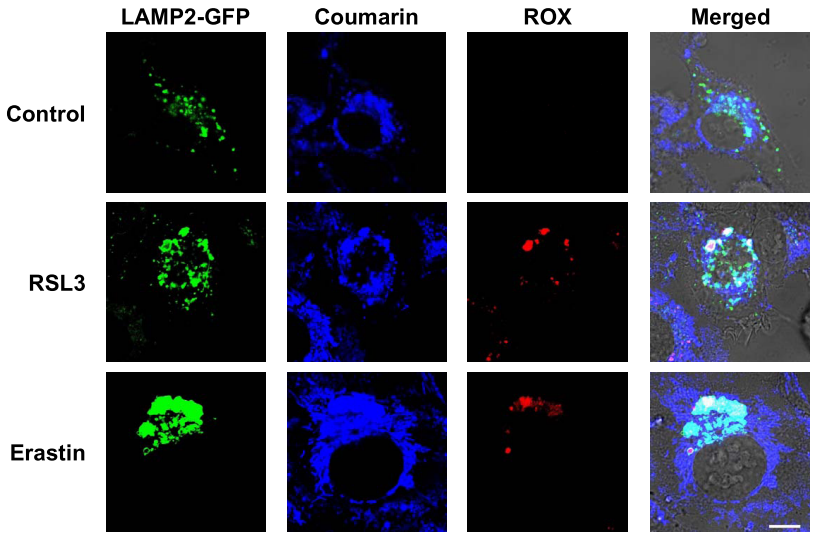

Figure 9. Lysosome-specific red fluorescence revealed in ferroptosis. **CALM**$^{+}$/LAMP2-GFP^{+} HT1080 cells were treated with no addition, with erastin (10 μM, 24 h), or with RSL3 (1 μM, 4 h) before confocal analysis. Scale bar: 10 μm.

https://doi.org/10.1021/acs.analchem.1c03881
Anal. Chem. 2021, 93, 16887−16898

ferroptosis. These results showed that **CALM**, overcoming the limitation of classical imaging agents prone to dissipation from dysfunctional mitochondria, is a powerful tool to track mitophagy and also to study mitochondrial biology.

■ ASSOCIATED CONTENT

Supporting Information

The Supporting Information is available free of charge at https://pubs.acs.org/doi/10.1021/acs.analchem.1c03881.

Synthesis and spectral analysis of new compounds, synthetic route for ^{DBCO}**RC-TPP**, selectivity and retention of the probe, imaging of mitophagy in additional cell lines with ^{DBCO}**RC-TPP**, and cytotoxicity of probes (PDF)

■ AUTHOR INFORMATION

Corresponding Author

Shoufa Han − *Department of Chemical Biology, College of Chemistry and Chemical Engineering, The Key Laboratory for Chemical Biology of Fujian Province, The MOE Key Laboratory of Spectrochemical Analysis & Instrumentation, and State Key Laboratory for Physical Chemistry of Solid Surfaces, Xiamen University, Xiamen 361005, China;* orcid.org/0000-0002-2057-0559; Phone: 86-0592-2181728; Email: shoufa@xmu.edu.en

Authors

Shixiong Wen − *State Key Laboratory of Cellular Stress Biology, School of Life Sciences, Xiamen University, Xiamen 361005, China*

Xiao Hu − *Department of Chemical Biology, College of Chemistry and Chemical Engineering, The Key Laboratory for Chemical Biology of Fujian Province, The MOE Key Laboratory of Spectrochemical Analysis & Instrumentation, and State Key Laboratory for Physical Chemistry of Solid Surfaces, Xiamen University, Xiamen 361005, China*

Yilong Shi − *State Key Laboratory of Cellular Stress Biology, School of Life Sciences, Xiamen University, Xiamen 361005, China*

Jiahuai Han − *State Key Laboratory of Cellular Stress Biology, School of Life Sciences, Xiamen University, Xiamen 361005, China*

Complete contact information is available at: https://pubs.acs.org/10.1021/acs.analchem.1c03881

Author Contributions

[§]S.W. and X.H. contributed equally to this work.

Notes

The authors declare no competing financial interest.

■ ACKNOWLEDGMENTS

This work was supported by grants from NSF China (22177096, 21775130, and 91854106). J.H. was supported by grants from NSF China (81788101).

■ REFERENCES

(1) Wang, L.; Qi, H.; Tang, Y.; Shen, H. M. *Trends Biochem. Sci.* **2020**, *45*, 58−75.
(2) Ashrafi, G.; Schwarz, T. L. *Cell Death Differ.* **2013**, *20*, 31−42.
(3) Kubli, D. A.; Gustafsson, A. B. *Circ. Res.* **2012**, *111*, 1208−1221.
(4) Panigrahi, D. P.; Praharaj, P. P.; Bhol, C. S.; Mahapatra, K. K.; Patra, S.; Behera, B. P.; Mishra, S. R.; Bhutia, S. K. *Semin. Cancer Biol.* **2020**, *66*, 45−58.
(5) Vives-Bauza, C.; Przedborski, S. *Trends Mol. Med.* **2011**, *17*, 158−165.
(6) Drake, L. E.; Springer, M. Z.; Poole, L. P.; Kim, C. J.; Macleod, K. F. *Semin. Cancer Biol.* **2017**, *47*, 110−124.
(7) Villa, E.; Marchetti, S.; Ricci, J. E. *Trends Cell Biol.* **2018**, *28*, 882−895.
(8) Malpartida, A. B.; Williamson, M.; Narendra, D. P.; Wade-Martins, R.; Ryan, B. J. *Trends Biochem. Sci.* **2021**, *46*, 329−343.
(9) Katayama, H.; Hama, H.; Nagasawa, K.; Kurokawa, H.; Sugiyama, M.; Ando, R.; Funata, M.; Yoshida, N.; Homma, M.; Nishimura, T.; Takahashi, M.; Ishida, Y.; Hioki, H.; Tsujihata, Y.; Miyawaki, A. *Cell* **2020**, *181*, 1176−1187.e16.
(10) Ye, Z.; Wei, L.; Geng, X.; Wang, X.; Li, Z.; Xiao, L. *ACS Nano.* **2019**, *13*, 11593−11602.
(11) Zhu, H.; Fan, J.; Du, J.; Peng, X. *Acc. Chem. Res.* **2016**, *49*, 2115−2126.
(12) Niu, G.; Liu, W.; Wu, J.; Zhou, B.; Chen, J.; Zhang, H.; Ge, J.; Wang, Y.; Xu, H.; Wang, P. *J. Org. Chem.* **2015**, *80*, 3170−3175.
(13) Liu, Y.; Zhou, J.; Wang, L.; Hu, X.; Liu, X.; Liu, M.; Cao, Z.; Shangguan, D.; Tan, W. *J. Am. Chem. Soc.* **2016**, *138*, 12368−12374.
(14) Tian, M.; Liu, C.; Dong, B.; Zuo, Y.; Lin, W. *Chem. Commun.* **2019**, *55*, 10440−10443.
(15) Lee, M. H.; Park, N.; Yi, C.; Han, J. H.; Hong, J. H.; Kim, K. P.; Kang, D. H.; Sessler, J. L.; Kang, C.; Kim, J. S. *J. Am. Chem. Soc.* **2014**, *136*, 14136−14142.
(16) Li, X.; Hu, Y.; Li, X.; Ma, H. *Anal. Chem.* **2019**, *91*, 11409−11416.
(17) Wang, X.; Fan, L.; Wang, S.; Zhang, Y.; Li, F.; Zan, Q.; Lu, W.; Shuang, S.; Dong, C. *Anal. Chem.* **2021**, *93*, 3241−3249.
(18) Zhang, W.; Kwok, R. T. K.; Chen, Y.; Chen, S.; Zhao, E.; Yu, C. Y. Y.; Lam, J. W. Y.; Zheng, Q.; Tang, B. Z. *Chem. Commun.* **2015**, *51*, 9022−9025.
(19) Iwashita, H.; Torii, S.; Nagahora, N.; Ishiyama, M.; Shioji, K.; Sasamoto, K.; Shimizu, S.; Okuma, K. *ACS Chem. Biol.* **2017**, *12*, 2546−2551.
(20) Huang, Z.; Li, N.; Zhang, X.; Wang, C.; Xiao, Y. *Anal. Chem.* **2018**, *90*, 13953−13959.
(21) Feng, G.; Liu, J.; Zhang, C.-J.; Liu, B. *ACS Appl. Mater. Interfaces* **2018**, *10*, 11546−11553.
(22) Leung, C. W. T.; Hong, Y.; Chen, S.; Zhao, E.; Lam, J. W. Y.; Tang, B. Z. *J. Am. Chem. Soc.* **2013**, *135*, 62−65.
(23) Chen, W.; Gao, C.; Liu, X.; Liu, F.; Wang, F.; Tang, L.-J.; Jiang, J.-H. *Anal. Chem.* **2018**, *90*, 8736−8741.
(24) Jin, C.; Liu, J.; Chen, Y.; Guan, R.; Ouyang, C.; Zhu, Y.; Ji, L.; Chao, H. *Sci. Rep.* **2016**, *6*, No. 22039.
(25) Shi, Y.; Zou, X.; Wen, S.; Gao, L.; Li, J.; Han, J.; Han, S. *Autophagy* **2021**, *17*, 3475−3490.
(26) Jao, C. Y.; Roth, M.; Welti, R.; Salic, A. *ChemBioChem* **2015**, *16*, 472−476.
(27) Tamura, T.; Fujisawa, A.; Tsuchiya, M.; Shen, Y.; Nagao, K.; Kawano, S.; Tamura, Y.; Endo, T.; Umeda, M.; Hamachi, I. *Nat. Chem. Biol.* **2020**, *16*, 1361−1367.
(28) Sletten, E. M.; Nakamura, H.; Jewett, J. C.; Bertozzi, C. R. *J. Am. Chem. Soc.* **2010**, *132*, 11799−11805.
(29) Song, X.; Bai, S.; He, N.; Wang, R.; Xing, Y.; Lv, C.; Yu, F. *ACS Sens.* **2021**, *6*, 1228−1239.
(30) Luo, X.; Wang, R.; Lv, C.; Chen, G.; You, J.; Yu, F. *Anal. Chem.* **2020**, *92*, 1589−1597.
(31) Wang, R.; Han, X.; You, J.; Yu, F.; Chen, L. *Anal. Chem.* **2018**, *90*, 4054−4061.
(32) Addanki, S.; Sotos, J. F. *Ann. N. Y. Acad. Sci.* **1969**, *147*, 756−804.
(33) Xue, Z.; Zhao, H.; Liu, J.; Han, J.; Han, S. *Anal. Chem.* **2017**, *89*, 7795−7801.
(34) Zhang, E.; Shi, Y.; Han, J.; Han, S. *Anal. Chem.* **2020**, *92*, 15059−15068.

(35) van Meer, G.; Voelker, D. R.; Feigenson, G. W. *Nat. Rev. Mol. Cell Biol.* **2008**, *9*, 112−124.
(36) Heytler, P. G. *Biochemistry* **1963**, *2*, 357−361.
(37) Sun, N.; Malide, D.; Liu, J.; Rovira, I. I.; Combs, C. A.; Finkel, T. *Nat. Protoc.* **2017**, *12*, 1576−1587.
(38) Cai, Q.; Jeong, Y. Y. *Cells* **2020**, *9*, No. 150.
(39) Liu, J.; Liu, W.; Li, R.; Yang, H. *Cells* **2019**, *8*, No. 712.
(40) Yoshimori, T.; Yamamoto, A.; Moriyama, Y.; Futai, M.; Tashiro, Y. *J. Biol. Chem.* **1991**, *266*, 17707−17712.
(41) Correia-Melo, C.; Ichim, G.; Tait, S. W. G.; Passos, J. F. *Nat. Protoc.* **2017**, *12*, 183−194.
(42) Yan, Y.; Zhang, X.; Zhang, X.; Li, N.; Man, H.; Chen, L.; Xiao, Y. *Chin. Chem. Lett.* **2020**, *31*, 1091−1094.
(43) Huang, Z.; Li, N.; Zhang, X.; Xiao, Y. *Anal. Chem.* **2021**, *93*, 5081−5088.
(44) Zhang, X.; Wang, L.; Li, N.; Xiao, Y. *Chin. Chem. Lett.* **2021**, *32*, 2395−2399.
(45) Tang, D.; Chen, X.; Kang, R.; Kroemer, G. *Cell Res.* **2021**, *31*, 107−125.
(46) Jiang, X.; Stockwell, B. R.; Conrad, M. *Nat. Rev. Mol. Cell Biol.* **2021**, *22*, 266−282.
(47) Wang, X.; Ma, H.; Sun, J.; Zheng, T.; Zhao, P.; Li, H.; Yang, M. *Biol. Trace Elem. Res.* **2021**, *200*, 298−307.
(48) Zhang, L.; Wang, F.; Li, D.; Yan, Y.; Wang, H. *Bioengineered* **2021**, *12*, 4983−4994.
(49) Basit, F.; van Oppen, L. M.; Schockel, L.; Bossenbroek, H. M.; van Emst-de Vries, S. E.; Hermeling, J. C.; Grefte, S.; Kopitz, C.; Heroult, M.; Hgm Willems, P.; Koopman, W. J. *Cell Death Dis.* **2017**, *8*, No. e2716.
(50) Chang, L. C.; Chiang, S. K.; Chen, S. E.; Yu, Y. L.; Chou, R. H.; Chang, W. C. *Cancer Lett.* **2018**, *416*, 124−137.
(51) Liu, M.; Fan, Y.; Li, D.; Han, B.; Meng, Y.; Chen, F.; Liu, T.; Song, Z.; Han, Y.; Huang, L.; Chang, Y.; Cao, P.; Nakai, A.; Tan, K. *Mol. Oncol.* **2021**, *15*, 2084−2105.
(52) Li, C.; Liu, J.; Hou, W.; Kang, R.; Tang, D. *Front. Cell Dev. Biol.* **2021**, *9*, No. 698679.
(53) Kang, R.; Tang, D. *Curr. Pathobiol. Rep.* **2017**, *5*, 153−159.
(54) Xie, Y.; Hou, W.; Song, X.; Yu, Y.; Huang, J.; Sun, X.; Kang, R.; Tang, D. *Cell Death Differ.* **2016**, *23*, 369−379.
(55) Liang, C.; Zhang, X.; Yang, M.; Dong, X. *Adv. Mater.* **2019**, *31*, No. e1904197.
(56) Nagai, S.; Yoshida, M.; Takigawa, Y.; Torii, S.; Koshiishi, I. *Food Chem.* **2021**, *343*, No. 128511.
(57) Torii, S.; Shintoku, R.; Kubota, C.; Yaegashi, M.; Torii, R.; Sasaki, M.; Suzuki, T.; Mori, M.; Yoshimoto, Y.; Takeuchi, T.; Yamada, K. *Biochem. J.* **2016**, *473*, 769−777.

https://doi.org/10.1021/acs.analchem.1c03881
Anal. Chem. 2021, 93, 16887−16898